Magnetic shielding in a planar geometry: using ferromagnetic washers to screen in-plane fields

Thomas Pirottin, Emile Fourneau, Alejandro V. Silhanek, Philippe Vanderbemden, and Benoît Vanderheyden

***Abstract*—Magnetic shielding is a crucial aspect for many electronic devices and sensors. In this paper, we investigate the magnetic shielding properties of ferromagnetic washers in a planar geometry in view of an integration with on-chip devices, focussing on the transverse configuration, i.e. with the applied field parallel to the plane of the washer. We show that, in this configuration, the shielding factor of a washer can exceed the predictions of previous studies. We argue that the magnetic shielding results from the capture of the external magnetic flux by the upper and lower faces of the washer, and its subsequent channeling through the washer material and around the central hole. We present experimental results and numerical simulations, and discuss the influence of the geometry of the washer, the permeability and the saturation of the ferromagnetic material. We propose an explanation for the observed behaviour and provide empirical formulae to estimate different quantities characterizing the shielding properties of washers in the transverse configuration.**

***Index Terms*—Magnetic shielding, planar geometry, ferromagnetic washer, ferromagnetic ring, on-chip, magnetic metamaterials**

I. Introduction

Many magnetic sensors and sensitive electronic devices need to operate in a well-known magnetic environment and thus require a protection against the earth magnetic field or stray magnetic fields produced by neighbouring circuits [1], [2], [3], [4]. For high frequency sources, a metallic enclosure with a thickness larger than the skin depth can provide the required shielding, thanks to the induced eddy currents. For low frequency sources (typically below 100 kHz), magnetic shielding at room temperature can be achieved with a high permeability ferromagnetic material that diverts magnetic flux from the sensitive region to be protected [5]. At low temperatures, superconducting materials can also be used to expel external magnetic flux away from their body and the sensitive area, due to their strong diamagnetic response. The magnetic flux penetration is limited by the Meissner effect for type-I superconductors [6] and, additionally, by flux pinning for irreversible type-II superconductors, [3], [7].

Besides the choice of the material, the efficiency of a magnetic shield is largely determined by its geometry. Particularly challenging geometries arise in situations where the specific part of a system requiring magnetic shielding has little clearance from the neighbouring elements. Other challenging situations are encountered in electronic circuits where a planar geometry is common and the magnetic shield needs to be designed with a limited footprint and volume. Such requirements arise in the design of magnetic memories [8], [9], where shielding against stray magnetic fields helps in reducing the bit error rate, as well as in high frequency transmission lines, where a magnetic screen may mitigate environmental fields, reduce crosstalk, and attenuate high frequency noise [10]. Last, such requirements also arise in superconducting circuits and sensors, where stray magnetic fields need to be reduced for the proper operation of Josephson junctions, SQUID devices, or transition edge sensors [3], [11].

Conventional ferromagnetic shielding configurations offer little help for building on-chip or volume-restricted devices in a planar geometry. The pioneering work of Mager [12] predicts very poor shielding abilities for highly permeable ferromagnetic flat rings, i.e. with a very small height h and a wall width w typically much smaller than the internal radius R_{in}, or $h \lesssim w \ll R_{\text{in}}$. Such a ring structure provides almost no field attenuation in the longitudinal configuration (i.e. when an external field is applied along the ring axis of symmetry), while attenuation of about a factor of 1.5 is predicted at its centre in the transverse configuration (i.e. when an external field is applied perpendicular to the ring axis). However, these previous studies seem to have concentrated on geometries for which the width w of the soft ferromagnetic material is much smaller than its other dimensions. Although the motivation for this width restriction appears to be for saving ferromagnetic material, it turns out that in a planar geometry, the shielding properties of *flat but wide-wall* rings (i.e. with $w \gtrsim R_{\text{in}}$), or *washers*, have been overlooked.

In this paper, we show that soft ferromagnetic washers can reach attenuation factors that exceed the predictions of previous studies when the external field is applied in the transverse configuration. The magnetic shielding results from the capture of the external magnetic flux by the wide area on the upper and lower faces of the washer, and its subsequent channeling through the washer material and around the central hole. Such properties give the possibility to use a ferromagnetic washer as a simple and inexpensive device for attenuating in-plane magnetic fields in planar geometries.

The manuscript is structured as follows: we first present the experimental setup in Section II and the finite element model used in Section III. A comparison of the experimental results with the numerical simulations is made in Sections IV-A and V-A. We then discuss further simulation results and propose an explanation for the observed behaviour in Sections IV-B and V-B. Initially, the impact of the geometry

T. Pirottin, P. Vanderbemden and B. Vanderheyden were with the Department of Electrical Engineering and Computer Science, Institut Montefiore B28, University of Liège, B-4000 Liège, Belgium.

E. Fourneau and A. V. Silhanek were with the Department of Physics, Experimental Physics of Nanostructured Materials, University of Liège, B-4000 Liège, Belgium.

of the washer and the permeability of the ferromagnetic material is discussed while ignoring the saturation effect. Then the impact of saturation of the ferromagnetic material is introduced. Empirical formulae are proposed to estimate different quantities characterizing the shielding properties of washers in Section IV-C and V-C. Finally, the generalization to the combination of multiple concentric washers is introduced in Section VI.

II. Experimental details

252.0pt

The shielding behaviour of ferromagnetic washers has been tested experimentally. A series of samples were submitted to a well-defined external magnetic field, and the resulting local magnetic field has been measured at different positions. The results are first shown in Section IV-A and further discussed in Section IV-B and Section V-B.

The samples were laser-cut from a 1 mm thick Mu-metal sheet, according to the geometry depicted in Fig. 1, where C marks the position of the centre, h is the height or thickness, R_{in} is the inner radius, R_{out} is the outer radius, and $w = R_{\text{out}} - R_{\text{in}}$ is the washer wall width. The Mu-metal used is a soft ferromagnetic material with negligible hysteresis. According to the manufacturer, this Mu-metal is an alloy of 80.0% nickel, 14.9% iron and 4.2% molybdenum, it has a low-field relative permeability $\mu_r = 30\,000$ and a saturation magnetic flux density $B_{\text{sat}} = 0.8$ T.

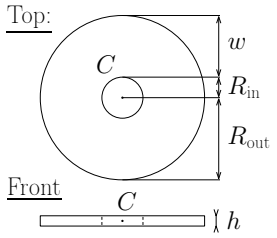

sample	h	R_{in}	w	R_{out}
S_1	1	5	1	6
S_2	1	5	5	10
S_3	1	5	15	20
S_4	1	5	45	50
S_5	1	5	95	100

Fig. 1. Schematic description of the washer geometry with the associated sample dimensions in millimetres.

The experimental setup is illustrated in Fig. 2. The external magnetic field is generated by a pair of split coils[1], fed with a current source and able to produce a maximum magnetic field of 3.95 mT at the centre of the setup. An Arepoc AXIS-3 Hall probe is used to measure the magnetic flux density. This probe consists of a long cylindrical casing with Hall sensors fitted at one end. It contains a Hall sensor capable of measuring the in-plane field in the configuration described in Fig. 2 with an active area of 50×50 µm^2. The probe is fixed on a 3-axis translation stage, which allows the measurement of the magnetic flux density to be made at different positions in the xyz-space close to the sample. A hole is made in the sample holder allowing the probe to pass through it and scan magnetic fields along the z-axis.

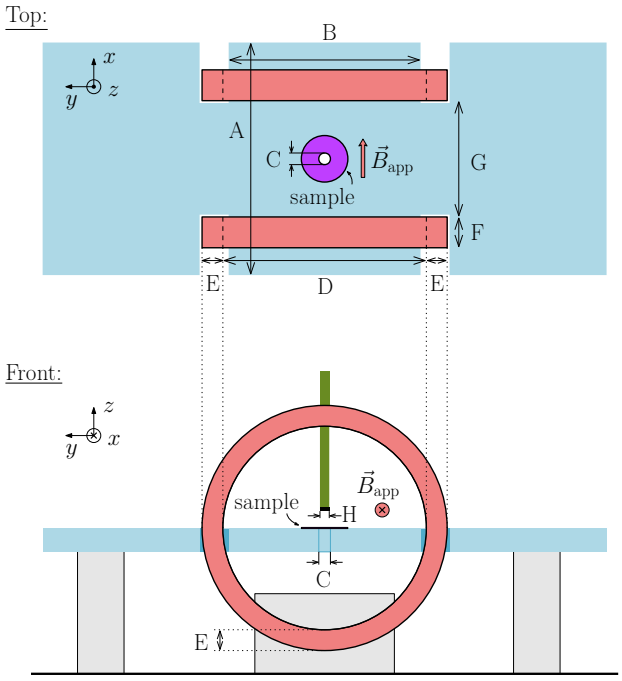

A	holder width	200
B	holder extent	165
C	holder hole diameter	10
D	coils inner diameter	175
E	coils width	18
F	coils thickness	26.5
G	coils spacing	100
H	sensor casing diameter	8

Fig. 2. Schematic of the experimental setup and its dimensions in millimetres. The sample holder is in blue, the coils are in red, the Hall probe sensor is in green and the fasteners are in grey.

Before starting the experimental measurement, a general calibration step is performed to align the applied field, the x-axis of the translation stage and the x-axis of the probe. The magnetic flux density at the centre of the setup is also measured at this step and is taken as the uniform applied field, $B_{\text{app}} \approx 3.95$ mT.

Then, the measurements can be performed by placing the samples in the centre of the sample holder, one at a time. The (x, y) coordinates of the centre of the sample are determined in order to centre the Hall probe above the hole of the sample. Finally, a series of measurements is taken at specific heights z_i, moving the probe along the z-axis. The goal of these measurements is to observe the decrease in magnetic flux density while approaching the centre of the washer, and measure the flux density at its centre.

III. Numerical model

Numerical simulations have been performed using finite element method on COMSOL Multiphysics® with the AC/DC

[1]The split coil geometry does not strictly conform with a Helmholtz configuration, as the distance between the coils is larger than their radius. As a result, the applied field varies in the vicinity of the center. However, for samples S_1-S_4, this variation is of the order of magnitude of the uncertainty brought by the physical realization of the experimental setup and the field sensor accuracy. A greater deviation is observed for S_5, however, a simulation with a uniform field $B_{\text{app}} = 3.95$ mT exhibits a B_x distribution that is similar to the one shown in Fig. 6, so that our conclusions on this sample are unaffected by the non-uniformity of the magnetic field.

module following two different approaches. First we consider the experimental conditions with a field generated by coils, in order to faithfully reproduce the experimental data. Second, a uniform field is used instead, in order to investigate the mechanisms at play while reducing the number of parameters to be varied. For this purpose, the shielding factor SF will be used to evaluate the shielding properties of a given configuration. The shielding factor is defined as

$$\mathrm{SF} = \frac{B_{\mathrm{app}}}{B_{\mathrm{centre}}}, \tag{1}$$

where B_{centre} is the component of the magnetic flux density parallel to the applied field and measured at the centre of the sample.

The constitutive law of the ferromagnetic material is approximated in two different ways. In a first approximation, the ferromagnetic material is considered to act as a linear magnetic material, with a fixed relative permeability. The obtained results are discussed in Section IV. In a second approximation, the saturation of the ferromagnetic material is taken into account, using a simple model for the magnetization curve $B(H)$. The obtained results are discussed in Section V.

IV. Analysis with a linear magnetic material

In this section, the simulations consider the ferromagnetic material as a linear magnetic material, i.e. a linear, isotropic, and homogeneous medium with a fixed relative permeability μ_{r}. Under this assumption, the flux density measured at the centre of the washer is a linear function of the applied field, making the shielding factor independent of it.

It is also interesting to notice that the results are invariant under a change of scale. This is due to the linearity of the Maxwell equations and of the considered constitutive law. It means that all washers with the same ratio $R_{\mathrm{out}}/R_{\mathrm{in}}$ and the same ratio h/R_{in} will exhibit the same shielding factor, when subjected to a fixed field that is uniform over the washer volume. Therefore, fixing a dimension for all considered geometries allows us to avoid redundancy in the results without overlooking any configuration. This has been done in simulations by fixing the inner radius $R_{\mathrm{in}} = 5$ mm for all washers, to match the inner radius of the experimental samples.

A. Results

The experimental results (symbols) are compared with simulations (continuous lines) in Fig. 3 for each of the samples of Fig. 1. For the simulations, a relative permeability $\mu_{\mathrm{r}} = 30\,000$ is considered in order to match the low-field relative permeability quoted by the manufacturer, and the applied field is generated by coils, as was done in the experiments.

For samples S_1-S_4, the experimental results show an attenuation of the in-plane component of the local magnetic field near the centre of the washer. The applied field intensity is gradually recovered as the probe moves vertically away from the washer centre. Both the intensity and the spatial extension of the attenuation increase as w increases. For instance, the attenuation of the in-plane component at the centre increases

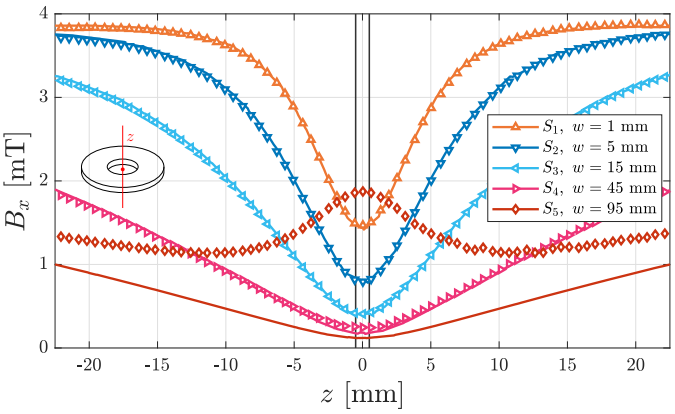

Fig. 3. Component of the magnetic flux density parallel to the applied field direction along the washer symmetry axis for different values of w. The symbols show experimental data, and the continuous lines show simulation results obtained with a fixed $\mu_r = 30\,000$. The two vertical lines mark the positions of respectively the bottom and top surfaces of the washers. Here, $R_{\mathrm{in}} = 5$ mm, $h = 1$ mm, $R_{\mathrm{out}} = R_{\mathrm{in}} + w$ and $B_{\mathrm{app}} = 3.95$ mT in the x-direction.

from 63 % of the applied field for $w = 1$ mm to 94 % for $w = 45$ mm, while half of the attenuation at the centre is reached over the area $|z| < 4.5$ mm for $w = 1$ mm against $|z| < 25.75$ mm for $w = 45$ mm. The lowest measured magnetic field at the centre is $B_{x,z=0} = 0.25$ mT with sample S_4, which corresponds to a shielding factor $\mathrm{SF} = B_{\mathrm{app}}/B_{x,z=0} = 16$. For sample S_5, although the measured curve exhibits an overall attenuation of B_x, a local increase is observed at the centre of the washer.

Simulations are in good agreement with the experimental data for the samples S_1-S_3. The simulations start to deviate from the experimental results for S_4 around $z = 0$ mm, where the measured field is found to be slightly larger than the simulated field ($< 2\%\, B_{\mathrm{app}}$ of difference). This discrepancy becomes more apparent with S_5, for which the measured field is significantly larger than the simulated field and exhibits a very different dependence as a function of z.

B. Discussion

The results of Fig. 3 show that a sizeable shielding factor can be obtained with a highly permeable ferromagnetic washer. A washer being the limiting case of a hollow cylinder whose height tends to zero, a deeper look at the magnetic shielding theory of ferromagnetic cylinders is in order. The theory developed by Mager [12] identifies two magnetic flux penetration routes in a soft ferromagnetic cylinder: a first one through the cylinder wall, as a fraction of the magnetic flux channelled in the ferromagnetic material around the inner cavity leaks into it, and a second one through the open ends. Assuming a ferromagnetic material of fixed relative permeability $\mu_{\mathrm{r}} \gg 1$ and neglecting edge effects, the associated shielding factors are given as

$$\mathrm{SF}_{\mathrm{wall}} = 1 + \frac{\mu_{\mathrm{r}}}{4}\left(1 - \left[\frac{R_{\mathrm{in}}}{R_{\mathrm{out}}}\right]^2\right), \tag{2}$$

$$\mathrm{SF}_{\mathrm{open}} = 1.5\,\exp\left(k_T\,\frac{h}{2R_{\mathrm{in}}}\right), \tag{3}$$

where $k_T = 3.832$ is the first zero of the Bessel function $J_1(x)$. The combination of these routes leads, by a simple addition of the two fields, to a net shielding factor

$$\mathrm{SF} = \left(\frac{1}{\mathrm{SF}_{\mathrm{wall}}} + \frac{1}{\mathrm{SF}_{\mathrm{open}}} \right)^{-1}. \tag{4}$$

Following these equations, the shielding factor of an infinitely thin cylinder ($h \to 0$) should tend towards $\mathrm{SF} \simeq \mathrm{SF}_{\mathrm{open}} \to 1.5$, and the shielding factor of a washer with $h = 1$ mm and $R_{\mathrm{in}} = 5$ mm, such as the experimental samples, should be limited by the shielding factor of its openings, i.e. $\mathrm{SF} \leq \mathrm{SF}_{\mathrm{open}} = 2.2$. Surprisingly, this limiting value is much lower than the value of $\mathrm{SF} = 16$ that was experimentally determined. Given the significant width of a washer wall in comparison to its height, edge effects are not negligible, and, therefore, Mager's theory [12] is not expected to hold for such geometries.

Indeed, Eq. (2) is obtained by considering the magnetic flux density channelled through the ferromagnetic material equivalent to that of an infinitely long cylinder. The equation is exact under this hypothesis. However, this magnetic flux density is impacted by the finite length of the cylinder, as magnetic flux above and below the ends of the cylinder is channelled into the ferromagnetic material as well. Some of this flux is captured by the top and bottom surfaces of the cylinder [13], [14], and by the outer side surface close to the top and bottom edges. This additional flux captured increases the flux density in the ferromagnetic material, mainly close to the top and bottom of the cylinder. In the case of a washer, the vicinity of the top and bottom surfaces is such that the additional flux captured increases the overall flux density in the ferromagnetic material. As this flux density increases, the intensity of the magnetic flux leaking into the hole close to the centre increases as well. This results in a lower $\mathrm{SF}_{\mathrm{wall}}$ than predicted by Eq. (2).

Eq. (3) is obtained considering long and very thin cylinders, making them somewhat equivalent to a cylindrical cavity subjected to the applied magnetic field at both ends. However, the actual field at the openings is further influenced by the ferromagnetic cylinder when it has a larger wall width. As explained above, magnetic flux above and below the ends of the cylinder is captured along the top and bottom surfaces of the cylinder. As a result, the magnetic flux density is expected to decrease near the openings of the cylinder, thus resulting in a higher $\mathrm{SF}_{\mathrm{open}}$ than predicted by Eq. (3). This effect is expected to be more pronounced when the wall width w is large compared to the other dimensions, as is the case for washers.

The impact of the edge effects on these two routes of field penetration highlights a competition between two phenomena: the increase of the magnetic flux inside the ferromagnetic material, and the decrease of the field close to the openings. Still ignoring the saturation of the ferromagnetic material, further simulations at fixed relative permeability are performed to better understand how these two phenomena balance themselves as a function of the width w of the washer. Fig. 4 shows the shielding factor for washers of fixed inner radius, for different values of relative permeability μ_{r} (Fig. 4.a) and different heights h (Fig. 4.b). The applied field is uniform and arbitrarily set to $B_{\mathrm{app}} = 1$ mT. The approximation curve (black lines) will be discussed in Section IV-C.

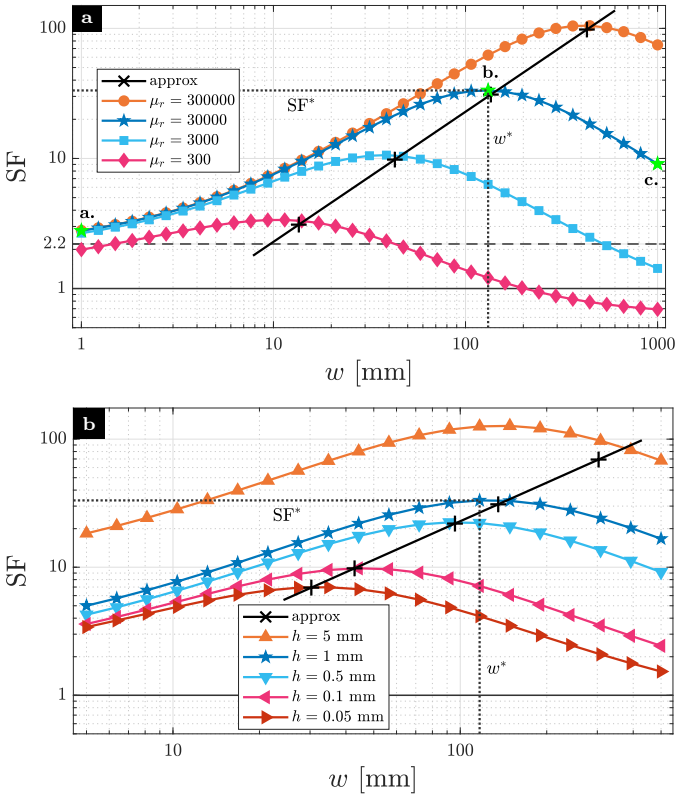

Fig. 4. Shielding factor as a function of the washer width w, (a) for different values of the relative permeability μ_{r} and $h = 1$ mm, (b) for different heights h and $\mu_{\mathrm{r}} = 30\,000$. Empirical approximation of the maximum of shielding factor SF* (5) and their corresponding width w^* (6) are represented by a black line for a continuous range of, respectively, μ_{r} and h, and by a cross for the simulation of specific values. For both panels, $R_{\mathrm{in}} = 5$ mm, $R_{\mathrm{out}} = R_{\mathrm{in}} + w$ and $B_{app} = 1$ mT. The horizontal line marks the limit between shielding ($\mathrm{SF} > 1$) and concentration ($\mathrm{SF} < 1$) of the field. The horizontal dashed line marks the prediction of $\mathrm{SF}_{\mathrm{open}}$ for $R_{\mathrm{in}} = 5$ mm and $h = 1$ mm according to Eq. (3). The three specific cases explored in Fig. 5 are marked with a green star on panel (a).

For a given μ_{r} and h, SF is seen to increase with w, reach a maximum SF* at a width w^*, and then decrease at larger widths. This maximum shielding factor (SF*) and its corresponding width (w^*) increase with μ_{r} and h. Note that for widths $w \gg w^*$, the shielding factor may decrease below 1, so that the magnetic flux density in the cavity is in fact *larger* than B_{app}, i.e. the magnetic flux is *concentrated* rather than shielded in the centre of the washer. For the sake of comparison, the shielding factor $\mathrm{SF}_{\mathrm{open}} = 2.2$ predicted by the theory of Mager [12] is also shown with a dashed line on Fig. 4.a. A significant improvement of the shielding factor above this theoretical result is observed for large μ_{r} and $w \sim w^*$.

Assuming that the two competing field penetration routes that were identified above are both reinforced by an increase of w, the behaviour of the shielding factor can be understood as follows. For $w < w^*$, the magnetic flux at the centre comes mainly from the openings. Since increasing w tends to decrease the field at the openings, this decreases the field

at the centre, and increases SF. For $w > w^*$, the magnetic flux at the centre results mainly from leaking through the ferromagnetic material. As increasing w tends to increase the magnetic flux density inside the ferromagnetic material, this increases the field leaking from it as well, and decreases SF. The maximum shielding factor SF* is reached when the changes coming from the two sources balance themselves. As an increase of μ_r allows channeling higher field intensity through the ferromagnetic material, and an increase of h allows a distribution of the additional flux captured by the top and bottom surfaces over a larger volume, an increase of either parameter reduces the magnetic flux leaking from the washer into the hole. As a result, the equilibrium between the two sources of magnetic flux is reached for larger w^* with a higher SF* when either μ_r or h is increased.

This explanation is relying on rough assumptions since the two phenomena are not evolving monotonically with w and they are difficult to quantify independently. Therefore, it is instructive to look at the magnetic field distribution close to the hole. The distribution of magnetic flux lines in the xz-plane is shown in Fig. 5 for washers of different widths w. The three panels respectively show cases with $w < w^*$ (a), $w \approx w^*$ (b), and $w > w^*$ (c), which are highlighted in Fig. 4.a as green stars. We should warn the reader that although the lines with arrows follow the actual magnetic flux lines, their surface density does not have any physical meaning. The intensity of the magnetic field should instead be deduced from the colour scale, which shows the ratio

$$\frac{B_\mathrm{app}}{\|\vec{B}(x, y = 0, z)\|}.$$

This colour scale can be understood as a map of the shielding level in the xz-plane, extending the definition of the shielding factor to other points than the centre. This choice is made to highlight the shielding level in the vicinity of the hole, and to better grasp the extent of the shielded region around it.

For $w < w^*$, Fig. 5.a, the magnetic flux lines filling the hole are coming from the openings. Moreover, some of the magnetic flux channelled around the hole by the ferromagnetic material is gathered by the inner side of the washer. This means that some flux lines penetrate the hole through the openings before entering the ferromagnetic material and being channelled around the hole. For $w \approx w^*$, Fig. 5.b, the magnetic flux lines filling the hole are still coming from the openings, but the magnetic flux gathered by the inner side of the washer is drastically reduced. The tendency is about to change, some flux lines escaping from the ferromagnetic material into the hole are about to appear after an additional increase in w. For $w > w^*$, Fig. 5.c, the flux lines inside the hole are leaking from the ferromagnetic material. Moreover, some flux is released by the top and bottom surfaces of the washer, close to the hole, passing above and below the openings without entering the hole. These observations are consistent with the above interpretation, showing a predominance of the flux coming from the openings for $w < w^*$, a predominance of the flux coming from the ferromagnetic material for $w > w^*$, and an intermediate state for $w \approx w^*$. Moreover, Fig. 5 gives additional information on the shape

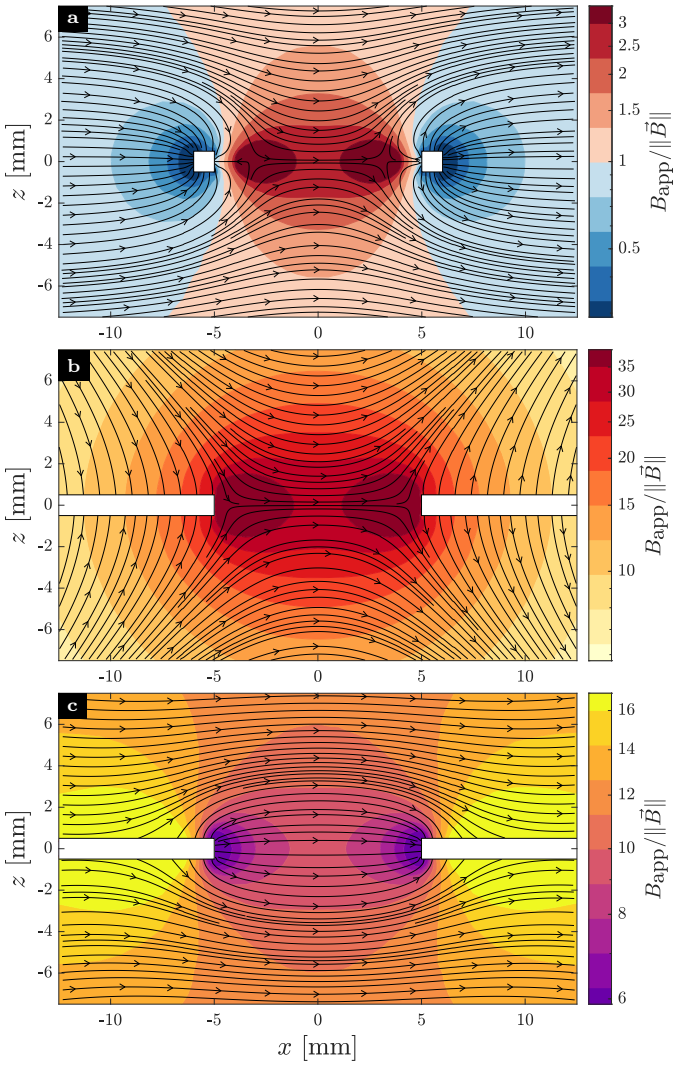

Fig. 5. Magnetic flux lines in the xz-plane for different values of w. Here, $R_\mathrm{in} = 5$ mm, $h = 1$ mm, $\mu_\mathrm{r} = 30\,000$, $B_{app} = 1$ mT, $w^* \simeq 131$ mm, $R^*_\mathrm{out} = w^* + R_\mathrm{in} \simeq 136$ mm. (a) $w = 1$ mm, $R_\mathrm{out} = 6$ mm, SF $= 2.8$. (b) $w = 131$ mm, $R_\mathrm{out} = 136$ mm, SF $= 33$. (c) $w = 1000$ mm, $R_\mathrm{out} = 1005$ mm, SF $= 9$.

of the magnetic field inside and around the hole, instead of focussing solely on the central point.

These three regimes are also different in terms of shielding performance. For $w < w^*$, the magnetic field cancels out at 2 points, symmetrically placed around the centre, on the line $\{y = 0; z = 0\}$. The shielding level decreases progressively around them. The shielded area is relatively small, extending a bit above and below the hole and growing with w. The area $\|\vec{B}\| < B_\mathrm{app}$ showing an attenuation of the magnetic field might be smaller than the hole if w is too small. This is actually the case in Fig. 5.a. For $w \approx w^*$, the 2 points where the field cancels out have moved towards the ferromagnetic material, almost to the point of merging with it. The shielded area is larger, engulfing the entire hole and extending all around it. The overall shielding level inside the hole is higher than for the other configurations. For $w > w^*$, the highest attenuation level is reached somewhere along the ferromagnetic material, where flux lines are tangent to its

surface. At these points, the flux density in the air is attenuated enough and the flux density inside the ferromagnetic material is strong enough to have a ratio between them equal to μ_r. The shielded area extends well around the hole, but a second area exhibiting a deterioration of the shielding level is growing inside the first, arising from the sides of the cavity. The larger the width w, the larger this second area, and the greater the deterioration of the shielding level. A region where the field is *concentrated*, i.e. $\|\vec{B}\| > B_{\text{app}}$, might appear in this second area if w is too large. If this region encloses the centre, this results in a SF < 1 as observed in Fig. 4.

The fitting in Fig. 3 confirms a good agreement between the above studied model and experiments, except for the largest sample width $w = 95$ mm. The samples S_1-S_4 are in the regime $w < w^*$, which explains that the magnetic field at the centre decreases and the shielded area around the hole increases as w increases. However, the change of behaviour of sample S_5 is not taken into account by the current model, which predicts a behaviour in the regime $w \approx w^*$. The model needs to be modified in order to better represent the behaviour of the ferromagnetic material. This is done in the following section, by taking the saturation of the ferromagnetic material into account.

C. Empirical formulae for the optimal width and shielding factor

It has been shown in Section IV-B that a washer of fixed inner radius and fixed height achieves a maximum of shielding factor SF* for a specific width w^*. The simulation results discussed in this section, as well as other simulation results not presented here, have been used to evaluate graphically SF* and w^*. The assumption is made that SF* and w^* follow a simple power law as a function of R_{in}, h and μ_r. The two following empirical formulae are obtained, and their predictions are compared with the simulation results in Fig. 4 (black line and crosses):

$$\text{SF}^* \simeq 0.4\sqrt{\frac{h\mu_r}{R_{\text{in}}}}, \tag{5}$$

$$w^* \simeq 0.35\sqrt{hR_{\text{in}}\mu_r}. \tag{6}$$

The empirical results fit well the simulation results in the cases where $\mu_r \gg 1$ and $h \ll R_{\text{in}}$, i.e. for thin washers made of high permeability ferromagnetic material. A ratio $h/R_{\text{in}} = 0.2$, corresponding to all curves in Fig. 4.a and the curve $h = 1$ mm in Fig. 4.b, results in a slight deviation of the empirical results, and a ratio $h/R_{\text{in}} = 1$, corresponding to the curve $h = 5$ mm in Fig. 4, results in a complete mismatch.

V. Analysis of the Saturation of the Ferromagnetic Material

The numerical model in the above section does not take into account the saturation of the ferromagnetic material, which is expected to occur in the experimental conditions and in real-world applications. In this section, the constitutive law linking the magnetic flux density B and the magnetic field strength H of the ferromagnetic material is changed from a constant relative permeability μ_r to an anhysteretic magnetization curve $B(H)$. An approximation of this magnetization curve taking saturation into account is given by the Frölich-Kennelly model [15], [16] where

$$\vec{B}(\vec{H}) = \left(\mu_0 + \left(\frac{1}{\mu_0\,(\mu_r - 1)} + \frac{\|\vec{H}\|}{\mu_0 M_{\text{sat}}}\right)^{-1}\right)\vec{H}, \tag{7}$$

with μ_0 the vacuum permeability (which also corresponds to the high field permeability), μ_r the low field relative permeability, and M_{sat} the saturated magnetization of the ferromagnetic material. In the following, simulations are performed using Eq. (7) with $\mu_r = 30\,000$ and $M_{\text{sat}} = 0.75/\mu_0$ A/m to match the properties of the Mu-metal used in the experiments.

A. Results

The experimental results (symbols) are compared with simulations (continuous lines) in Fig. 6. The simulations consider the $B(H)$ saturation curve expressed by Eq. (7), and an applied field generated by coils to match the experimental conditions.

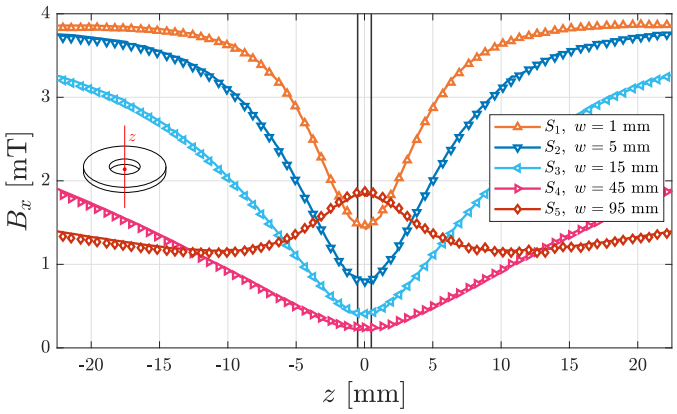

Fig. 6. In-plane component of the magnetic flux density along the washer symmetry axis for different values of w. The symbols show experimental data, and the continuous lines show simulation results obtained with the $B(H)$ curve expressed by Eq. (7). The two vertical lines mark the positions of respectively the bottom and top surfaces of the washers. Here, $R_{\text{in}} = 5$ mm, $h = 1$ mm, $R_{\text{out}} = R_{\text{in}} + w$ and $B_{\text{app}} = 3.95$ mT in the x-direction.

The experimental results are those presented in Fig. 3. Simulations are now in good agreement with the experimental data for all samples.

B. Discussion

A comparison of the results of Fig. 3 and Fig. 6 show that both representations of the ferromagnetic-material constitutive law yield similar results for samples S_1-S_4, meaning that saturation has a minimal effect on these samples, while saturation must be taken into account to explain the behaviour of sample S_5. To shed light on the impact of saturation on the shielding factor, further simulations including saturation are performed for washers of fixed geometries under an increasing applied field amplitude. Indeed, saturation limits the magnetic response of the ferromagnetic material when the magnetic field amplitude exceeds a certain level, and the magnetic field

level inside the ferromagnetic material for a given geometry increases with the applied field. The results are shown in Fig. 7 for a uniform applied field and washers with the dimensions of the experimental samples.

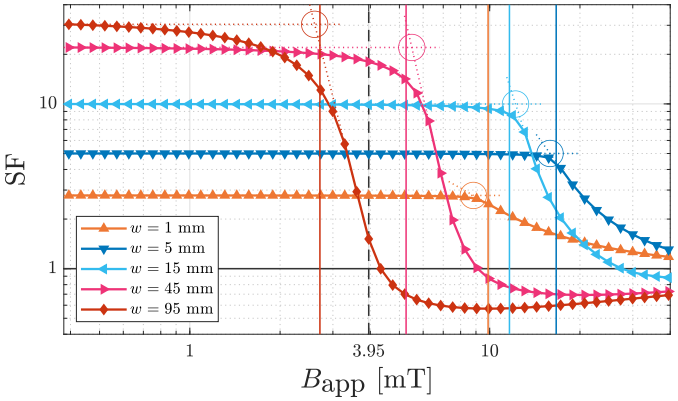

Fig. 7. Shielding factor as a function of the applied field amplitude for different w. Circles show the graphical evaluation of $B_{\text{app,th}}$ while vertical lines show the approximation of $B_{\text{app,th}}$ evaluated by (8). The horizontal line marks the limit between shielding (SF $>$ 1) and concentration (SF $<$ 1) of the field. The dashed vertical line represents the amplitude of the experimental applied field. Here, $R_{\text{in}} = 5$ mm, $h = 1$ mm, $R_{\text{out}} = R_{\text{in}} + w$, and the saturation curve $B(H)$ expressed by Eq. (7) is used.

It can be seen in Fig. 7 that the shielding factor of each geometry is almost constant for low amplitudes of the applied field. This shielding factor corresponds to the one obtained with the previous model, ignoring saturation. Then, a drop of the shielding factor occurs due to saturation. Finally, the shielding factor reaches a minimum value below 1, meaning that the magnetic field is *concentrated* in the hole of the washer for this applied field amplitude, before increasing slowly at higher applied field amplitudes, as the shielding factor tends asymptotically towards 1 due to the finite magnetization of the ferromagnetic material. The drop of shielding factor happens at different applied field amplitudes depending on the geometry of the washer. The threshold of applied field amplitude $B_{\text{app,th}}$, marking the onset of the drop, is found graphically as the intersection between a horizontal line tangent to the curve at low applied field and the tangent passing by the inflection point, i.e. the steepest tangent to the curve. The points obtained by this method are circled in Fig. 7 and correspond to a graphical approximation of the applied field amplitude at which saturation occurs in the ferromagnetic material for each geometry. The approximation of $B_{\text{app,th}}$ represented by vertical lines will be discussed in Section V-C.

The applied field amplitude of the experiment is represented on Fig. 7 by a dashed line. It crosses the curve for $w = 95$ mm when the shielding factor has already dropped significantly from its initial value, while it crosses the other curves before their drop. This confirms that the ferromagnetic material of sample S_5, with a width $w = 95$ mm, was saturated during the experiment. Figure 8 shows the modelled magnetization M and the relative permeability $\mu/\mu_0 = B/\mu_0 H$ of the ferromagnetic material of this last washer for a magnetic flux density $B_{\text{app}} = 3.95$ mT applied along the x-axis.

The magnetization level shown in Fig. 8 allows to highlight

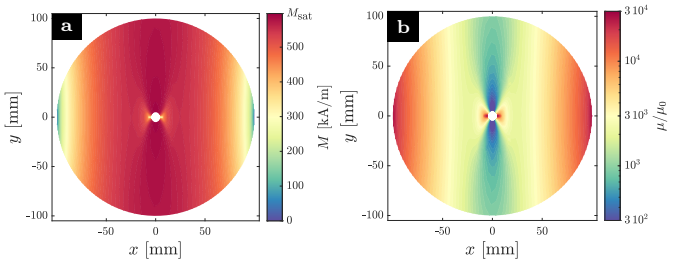

Fig. 8. Magnetization M (a) and relative permeability μ/μ_0 (b) of the ferromagnetic material in the xy-plane. Here, $R_{\text{in}} = 5$ mm, $h = 1$ mm, $w = 95$ mm, $R_{\text{out}} = 100$ mm, $\mu = B/H$ following the $B(H)$ curve expressed by Eq. (7), and $B_{\text{app}} = 3.95$ mT.

the saturated area, i.e. with $M \sim M_{\text{sat}}$, in red on the graph. This relatively large area extends from the hole to the sides along the y-axis, then spreads out towards the front and back ends with decreasing levels of magnetization. The relative permeability $B/\mu_0 H$ of the ferromagnetic material, displayed in Fig. 8.b, shows how saturation deteriorates the ferromagnetic properties of the washer. The relative permeability is at its lowest level along the y-axis, more specifically at the two sides of the hole, where the saturation is most critical. Indeed, the magnetic flux is caught progressively from the front end of the washer, and progressively released at its back end, explaining that the magnetic field concentration increases while getting closer to the y-axis. On top of that, the deviation of the magnetic flux around the hole increases further the magnetic field at its sides.

The working principle of the washer is to channel the magnetic flux lines in the ferromagnetic material to deviate them from the hole. This relies on the low reluctance paths around the hole offered by the high permeability of the ferromagnetic material. A decrease in this magnetic permeability, due to saturation, reduces the efficiency of these paths. The flux collected by the front end of the washer is less efficiently channelled while crossing the y-axis, more flux lines cross the y-axis through the air, and, therefore, through the hole, and the shielding factor decreases due to saturation.

A non-monotonic evolution of the threshold field $B_{\text{app,th}}$ is observed as a function of the width w. For small widths, $w < 5$ mm, $B_{\text{app,th}}$ increases with w. The low reluctance paths around the hole are relatively thin and can only channel a limited amount of magnetic flux before being saturated due to their limited size. Therefore, a smaller width results in narrower paths, leading to a lower $B_{\text{app,th}}$. On the other hand, for larger widths, $w > 5$ mm, $B_{\text{app,th}}$ decreases with w. As discussed before, an increase in w results in a greater overall concentration of the magnetic field in the ferromagnetic material, leading to a lower $B_{\text{app,th}}$.

C. Approximate formula for the threshold field

If the formulae obtained in Section IV-C can be used to optimize the shape of a washer and estimate the resulting shielding factor, it is also important to take saturation into account. In Section V-B, it was shown that the strength of the applied field leading to saturation depends on the washer dimensions. As shown in Appendix A, the threshold magnetic

flux density at which SF exhibits a sudden drop can be approximated as

$$B_{\text{app,th}} \simeq \mu_0 \left(1 + N_1 \mu_\text{r}\right) \left(1 - N_2\right) \left(1 - \left[\frac{R_\text{in}}{R_\text{out}}\right]^{1.5}\right) \frac{M_\text{sat}}{\mu_\text{r}}, \tag{8}$$

where N_1 and N_2 are the transverse demagnetizing factors of spheroids with respective aspect ratios $\gamma = h/2R_\text{out}$ and $\gamma = h/2R_\text{in}$, M_sat is the saturated magnetization of the ferromagnetic material, and μ_r is the low-field relative permeability of the ferromagnetic material. This approximation is in very good agreement with the simulation results, as shown in Fig. 7 (vertical lines).

VI. Combination of Multiple Concentric Washers

Studies on infinitely long cylinders have considered the combination of concentric cylinders of fixed permeability [12]. Such multi-layer structures can provide a higher shielding factor than a single cylinder with the same volume of material and the same inner radius. This section aims to extend this well-known result to washers.

We will consider the case of two concentric washers with the same height and compare it to a single washer with the same volume of material. The single washer has the dimensions of S_5, while the two washers are separated by a gap arbitrarily set to 1 mm. The material is assumed to be linear, isotropic and homogeneous, like in Section IV, with a fixed relative permeability $\mu_\text{r} = 30\,000$. The amplitude of the magnetic flux density and the distribution of magnetic flux lines in the ferromagnetic material are shown in Fig. 9 in the xy-plane of symmetry for both configurations. The simulations also showed a significant increase of the shielding factor due to the presence of the gap, passing from SF $= 32$ for the single washer to SF $= 50$ for the two washers.

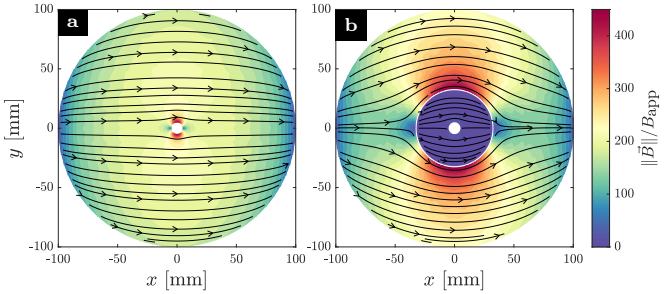

Fig. 9. Magnetic flux lines in the xy-plane of symmetry. (a) Single washer with $R_\text{in} = 5$ mm, $h = 1$ mm, $w = 95$ mm, $R_\text{out} = 100$ mm and $\mu_\text{r} = 30\,000$, leading to SF $= 32$ at the centre. (b) Two washers separated by a 1 mm gap, with $h = 1$ mm and $\mu_\text{r} = 30\,000$, leading to SF $= 50$ at the centre and keeping the same total volume of material as in (a). The inner washer covers a tenth of the total volume with $R_\text{in} = 5$ mm, $w = 27$ mm, $R_\text{out} = 32$ mm, and the outer washer covers the remaining volume with $R_\text{in} = 33$ mm, $w = 67.3$ mm, $R_\text{out} = 100.3$ mm.

The field lines in the single washer, Fig. 9.a, are mainly aligned with the applied field, i.e. along the x-direction. The amplitude of the magnetic flux density increases progressively from the front end of the washer to the y-axis. The magnetic flux is then deviated in the vicinity of the hole, creating 2 critical zones of high amplitude of the magnetic flux density on its sides. In the second configuration, Fig. 9.b, the ratio between the width and the inner radius of the outer washer is largely reduced compared to the single washer. This results in more pronounced critical zones, covering a larger area and showing slightly higher amplitudes of magnetic flux density. However, these critical zones are further away from the centre as the inner radius of the outer washer is larger. Moreover, the field lines are less aligned with the applied field in favour of the azimuthal direction, with the flux captured by the front end of the outer washer diverted around the hole further away from it. The inner washer shows very low amplitudes of magnetic flux density compared to both the outer washer and the single washer.

The low amplitude of magnetic flux density in the inner washer partly explains the increase in the shielding factor in the two-washer configuration. Indeed, as the flux density is reduced in the ferromagnetic material close to the hole, the flux leaking from it into the hole will be reduced as well. However, the improvement of the shielding factor obtained by dividing a washer in two separate pieces is less pronounced when the original washer has a small wall width, since in this case the magnetic flux in the hole comes mainly from the openings.

Here, the widest experimental sample has been chosen as the single washer geometry, the gap width has been arbitrarily set to the height of the washers, and the volume ratio between the inner and outer washers has been chosen as $1:9$. Reducing the volume of the inner washer would bring the critical zones of the outer washer closer to the centre, while increasing the volume of the inner washer would reduce the magnetic flux diverted by the outer washer. The chosen ratio seems to be a good trade-off.

To consider the effect of saturation on the two washers, the same assumptions as in Section V are made, using the $B(H)$ constitutive law described by Eq. (7). The resulting modelled shielding factors are shown in Fig. 10. As observed above, the outer washer has thinner arms for a slightly larger outer radius than the single washer resulting in more pronounced critical zones, and the inner washer shows a reduced magnetic flux density. Therefore, the threshold of applied field amplitude above which saturation occurs is lower for the outer washer and higher for the inner washer than for the single washer. It can be noted that Eq. (8) can be used to approximate the threshold associated to the outer washer.

The presence of two thresholds of applied field amplitude with two washers results in three regimes of applied field amplitude: a first linear regime where the shielding factor is constant, a second regime where the shielding factor decreases moderately due to saturation in the outer washer, and a third regime where the shielding factor drops significantly due to saturation in the inner washer. In comparison to the single washer, the linear range where the shielding factor is nearly constant is reduced as the outer washer threshold is lower than the single washer one, whereas the range of applied field leading to a sizeable shielding factor is increased as the inner washer threshold is higher than the single washer one. Overall, the shielding factor is higher with two washers than with a single one.

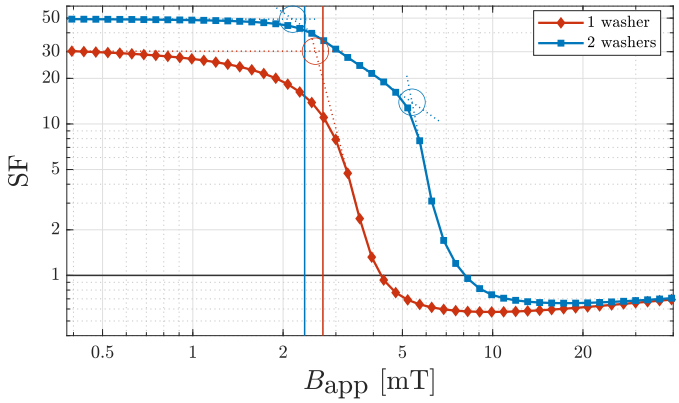

Fig. 10. Shielding factor as a function of the applied field amplitude for a single washer and two concentric washers. Circles show the graphical evaluation of the threshold of applied field amplitude of the different washers, while the vertical lines show the approximation of these thresholds evaluated by Eq. (8). The horizontal line marks the limit between shielding (SF > 1) and concentration (SF < 1) of the field. Here, $h = 1$ mm and the saturation curve $B(H)$ expressed by Eq. (7) is used, with $R_{\text{in}} = 5$ mm, $w = 95$ mm and $R_{\text{out}} = 100$ mm for the single washer, $R_{\text{in}} = 5$ mm, $w = 27$ mm and $R_{\text{out}} = 32$ mm for the inner washer, and $R_{\text{in}} = 33$ mm, $w = 67.3$ mm and $R_{\text{out}} = 100.3$ mm for the outer washer.

VII. Conclusion

It has been shown both experimentally and numerically that a sizeable attenuation of a transverse applied field can be obtained using a ferromagnetic washer. A first study ignoring the saturation of the ferromagnetic material has highlighted the presence of a maximum shielding factor, varying as a function of the width of the washer. Empirical formulae have been presented to evaluate w^* and its associated SF*. Then, the influence of the saturation has been explored. It has been shown that saturation impacts negatively the shielding efficiency of the washer. This translates into an upper limit of the applied field amplitude that a washer can shield, and a formula has been presented to evaluate this threshold value. Finally, the generalization to multiple concentric washers has been introduced with a particular case study.

Further investigations are needed to study the magnetic behaviour of washers under time varying applied fields and the impact of hysteresis on the shielding factor. Also, a more thorough study of structures with multiple washers is needed to better optimize the various geometric parameters involved. Moreover, this can be the starting point to adapt the concepts of magnetic metamaterial devices [17], [18] to a planar geometry. Indeed, such structures should exhibit an anisotropic behaviour, with an azimuthal permeability larger than the radial one. The studied concentric washers show a similar anisotropy, as the presence of the gap impedes the channeling of the magnetic flux along the radial direction.

Finally, the possibility of using washers to attenuate in-plane fields offers interesting perspectives for on-chip applications. The washers studied in this paper could be miniaturized to obtain washers with an external radius of tens of micrometres, a scale at which the magnetic response will be largely dependent on the dynamics of magnetic domains. The response of such structures will be the object of future work.

Appendix A
Derivation of the Threshold Field

In this appendix, an approximate expression is established for the threshold field $B_{\text{app,th}}$, i.e. the applied field for which the washer material starts saturating. The approximation is based on the analytical expression for the perturbation of a uniform, parallel field applied on a dielectric spheroid, derived in Stratton's classical textbook [19]. This problem can be directly translated into that of the perturbation of a uniform field due to a magnetic spheroid by replacing electric fields by magnetic fields and permittivities by permeabilities.

Consider first the case of a spheroid of semiaxes a, b, and c, with $a = b > c$. The spheroid has a permeability μ_1 and is embedded in a homogeneous medium of permeability μ_2. For an applied field that is uniform and directed along one of the semiaxes of length a (say, along the x-axis), the magnetic field inside the spheroid is uniform and given as

$$H_{\text{in,x}} = \frac{H_{\text{app}}}{1 + N\left(\frac{\mu_1}{\mu_2} - 1\right)}, \tag{9}$$

where N, the demagnetization factor, is a function of the ratio $\gamma = c/a \leq 1$,

$$N(\gamma) = \frac{a^2 c}{2} \int_0^\infty \frac{ds}{(s + a^2)^2 \sqrt{s + c^2}}, \tag{10}$$

$$= \frac{\gamma}{2\,(1 - \gamma^2)} \left(\frac{\arccos \gamma}{\sqrt{1 - \gamma^2}} - \gamma \right). \tag{11}$$

Next, consider a washer of height h, outer radius R_{out}, and inner radius R_{in}. The washer material has a permeability $\mu = \mu_{\text{r}}\mu_0$, is placed in vacuum and is subjected to a uniform field H_{app} applied along the x-direction. The field inside the hole is approximated in two steps. In the first step, the washer geometry is approximated by a solid spheroid with $a = R_{\text{out}}$ and $c = h/2$. From Eq. (9) with $\mu_1/\mu_2 = \mu_{\text{r}}$, the magnetic field inside the spheroid is given as

$$H_{\text{washer}} = \frac{H_{\text{app}}}{1 + N_1(\mu_{\text{r}} - 1)}, \tag{12}$$

where $N_1 = N(\gamma_1)$ with $\gamma_1 = h/2R_{\text{out}}$. In the second step, consider a spheroidal cavity with $a = R_{\text{in}}$ and $c = h/2$, hollowed out of the larger solid spheroid, in its centre. Assuming the cavity is immersed in a field that can be approximated by the uniform field of Eq. (12) and applying Eq. (9) with $\mu_2/\mu_1 = \mu_{\text{r}}$, one has

$$H_{\text{cavity}} = \frac{H_{\text{washer}}}{1 + N_2\left(\frac{1}{\mu_{\text{r}}} - 1\right)}. \tag{13}$$

In order to determine the threshold field leading to saturation, one observed in Section IV-C that the magnetization starts saturating to M_{sat} along the lateral surface of the washer hole, in a plane perpendicular to the applied field. Thus, by continuity of the tangential component of the magnetic field, the surface magnetic field in the washer hole will be equal to $H_{\text{sat}} = M_{\text{sat}}/(\mu_{\text{r}} - 1)$. Going back to the two approximations in Eq. (12) and (13), assuming $H_{\text{cavity}} \simeq H_{\text{sat}}$, one finds

$$B_{\text{app,th}} \approx \mu_0 \left(1 + N_1(\mu_{\text{r}} - 1)\right) \left(1 + N_2 \left(\frac{1}{\mu_{\text{r}}} - 1\right)\right) \frac{M_{\text{sat}}}{\mu_{\text{r}} - 1}. \tag{14}$$

In practice, it turns out this approximation works well as long as $R_{\text{in}}/R_{\text{out}} \ll 1$. For larger ratios, we found empirically that multiplying $B_{\text{app,th}}$ by a factor $1-(R_{\text{in}}/R_{\text{out}})^{1.5}$ provides a better fit, leading to the final expression

$$\begin{aligned} B_{\text{app,th}} &\simeq \mu_0\left(1+N_1\left(\mu_{\text{r}}-1\right)\right)\left(1+N_2\frac{1-\mu_{\text{r}}}{\mu_{\text{r}}}\right) \\ &\quad \left(1-\left[\frac{R_{\text{in}}}{R_{\text{out}}}\right]^{1.5}\right)\frac{M_{\text{sat}}}{\mu_{\text{r}}-1}, \\ &\approx \mu_0\left(1+N_1\mu_{\text{r}}\right)\left(1-N_2\right) \\ &\quad \left(1-\left[\frac{R_{\text{in}}}{R_{\text{out}}}\right]^{1.5}\right)\frac{M_{\text{sat}}}{\mu_{\text{r}}}, \quad (\mu_{\text{r}} \gg 1), \end{aligned} \tag{15}$$

which was introduced in Section IV-C.

ACKNOWLEDGMENT

The authors gratefully acknowledge the financial support from the Fonds de la recherche Scientifique - FNRS, Belgium under the grants of project PDR T.0204.21 and EraNet-CHIST-ERA R.8003.21. The work of E. Fourneau has been financially supported by the FWO and F.R.S.-FNRS under the Excellence of Science (EOS) project O.0028.22.

REFERENCES

[1] K. Kamiya, B. Warner, and T. Numazawa, "Geometry Dependence of Superconducting Shielding for Sensitive Detectors," *IEEE Transactions on Appiled Superconductivity*, vol. 14, no. 2, pp. 1042–1045, Jun. 2004.

[2] Weizhong Wang and Zhenye Jiang, "Magnetic Shielding Design for Magneto-Electronic Devices Protection," *IEEE Transactions on Magnetics*, vol. 44, no. 11, pp. 4175–4178, Nov. 2008.

[3] Y. Ishisaki, H. Kurabayashi, A. Hoshino, T. Ohashi, T. Yoshino, T. Hagihara, K. Mitsuda, and K. Tanaka, "Effect of On-Chip Magnetic Shielding for TES Microcalorimeters," *Journal of Low Temperature Physics*, vol. 151, no. 1-2, pp. 131–137, Apr. 2008.

[4] J. M. Kreikebaum, A. Dove, W. Livingston, E. Kim, and I. Siddiqi, "Optimization of infrared and magnetic shielding of superconducting TiN and Al coplanar microwave resonators," *Superconductor Science and Technology*, vol. 29, no. 10, p. 104002, Oct. 2016.

[5] C. R. Paul, R. C. Scully, and M. A. Steffka, *Introduction to electromagnetic compatibility*, 3rd ed. Hoboken, NJ: Wiley, 2023.

[6] M. Tinkham, *Introduction to superconductivity*, 2nd ed., ser. Dover books on physics. Mineola, NY: Dover Publ, 2015.

[7] S. Denis, G. Grenci, L. Dusoulier, R. Cloots, P. Vanderbemden, B. Vanderheyden, M. Dirickx, and M. Ausloos, "Characterisation of the magnetic shielding properties of YBaCuO thick films prepared by electrophoretic deposition on silver substrates," *Journal of Physics: Conference Series*, vol. 43, pp. 509–512, Jun. 2006.

[8] T. Watanabe and S. Yamamichi, "A novel U-shaped magnetic shield for perpendicular MRAM," in *2012 IEEE 62nd Electronic Components and Technology Conference*. San Diego, CA, USA: IEEE, May 2012, pp. 920–925.

[9] B. Bhushan, L. T. Guan, D. Shum, E. W. L. Ching, B. Y. Jung, W. Y. Lim, W. Yi, F. Poh, and J. B. Tan, "Enhancing Magnetic Immunity of STT-MRAM with Magnetic Shielding," in *2018 IEEE International Memory Workshop (IMW)*. Kyoto: IEEE, May 2018, pp. 1–4.

[10] J. Ma, S. Muroga, Y. Endo, S. Hashi, M. Naoe, H. Yokoyama, Y. Hayashi, and K. Ishiyama, "Noise suppression and crosstalk analysis of on-chip magnetic film-type noise suppressor," *AIP Advances*, vol. 8, no. 5, p. 056613, May 2018.

[11] R. S. Bakolo, R. Van Staden, P. Febvre, and C. J. Fourie, "Modelling Magnetic Fields and Shielding Efficiency in Superconductive Integrated Circuits," *Journal of Superconductivity and Novel Magnetism*, vol. 30, no. 6, pp. 1649–1653, Jun. 2017.

[12] A. Mager, "Magnetic shields," *IEEE Trans. Magn.*, vol. 6, no. 1, pp. 67–75, 1970.

[13] N. Bort-Soldevila, J. Cunill-Subiranas, A. Barrera, N. Del-Valle, A. V. Silhanek, V. Uhlíř, S. Bending, A. Palau, and C. Navau, "Enhanced magnetic field concentration using windmill-like ferromagnets," *APL Materials*, vol. 12, no. 2, p. 021123, Feb. 2024.

[14] N. Lejeune, E. Fourneau, A. Barrera, O. Morris, O. Leonard, J. A. Arregi, C. Navau, V. Uhlíř, S. Bending, A. Palau, and A. V. Silhanek, "Dimensional Crossover of Microscopic Magnetic Metasurfaces for Magnetic Field Amplification," 2024, version Number: 1.

[15] A. E. Kennelly, "Magnetic Reluctance," *Transactions of the American Institute of Electrical Engineers*, vol. VIII, no. 1, pp. 483–533, Jan. 1891.

[16] R. M. Bozorth, "The Magnetization Curve and the Domain Theory," in *Ferromagnetism*. IEEE, 1978, ch. 11.

[17] J. Prat-Camps, A. Sanchez, and C. Navau, "Superconductor–ferromagnetic metamaterials for magnetic cloaking and concentration," *Superconductor Science and Technology*, vol. 26, no. 7, p. 074001, Jul. 2013.

[18] A. Sanchez, C. Navau, J. Prat-Camps, and D.-X. Chen, "Antimagnets: controlling magnetic fields with superconductor–metamaterial hybrids," *New Journal of Physics*, vol. 13, no. 9, p. 093034, sep 2011.

[19] J. A. Stratton, *Electromagnetic Theory*, 1st ed. McGraw-Hill Companies (New York), 1941.